Stem Cell Research & Therapy

RESEARCH

Open Access

3D spheroids versus 2D-cultured human adipose stem cells to generate smooth muscle cells in an internal anal sphincter-targeting cryoinjured mouse model

Iltae Son[1,2*], Minsung Kim[1], Ji-Seon Lee[3], Dogeon Yoon[3], You-Rin Kim[3], Ji Hye Park[3], Bo-Young Oh[1], Wook Chun[4] and Sung-Bum Kang[5*]

Abstract

Background The efficacy of cell implantation via 3D-spheroids to treat basal tone in fecal incontinence remains unclear. To address this, in this study, we aimed to identify cell differentiation and assess the development of a contractile phenotype corresponding to smooth muscle cells (SMCs) following implantation of 3D-spheroid and 2D-cultured human adipose stem cells (hASCs) in an in vivo internal anal sphincter (IAS)-targeted mouse model.

Methods We developed an IAS-targeted in vivo model via rapid freezing (at − 196 °C) of the dorsal layers of the region of interest (ROI) of the IAS ring posterior quarter, between the submucosal and muscular layers, following submucosal dissection (n = 60 rats). After implantation of tetramethylindocarbocyanine perchlorate (DiI)-stained 3D and 2D-cells into randomly allocated cryoinjured rats, the entire sphincter ring or only the cryoinjured ROI was harvested. Expression of SMC markers, RhoA/ROCKII and its downstream molecules, and fibrosis markers was analyzed. DiI, α-smooth muscle actin (α-SMA), and RhoA signals were used for cell tracking.

Results In vitro, 3D-spheroids exhibited higher levels of SMC markers and RhoA/ROCKII-downstream molecules than 2D-hASCs. The IAS-targeted cryoinjured model exhibited substantial loss of SMC layers of the squamous epithelium lining of the anal canal, as well as reduced expression of SMC markers and RhoA-related downstream molecules. In vivo, 3D-spheroid implantation induced SMC markers and contractile molecules weakly at 1 week. At 2 weeks, the mRNA expression of *aSma, Sm22a,* Smoothelin, *RhoA, Mypt1, Mlc*$_{20}$, *Cpi17,* and *Pp1cd* increased, whereas that of fibrosis markers reduced significantly in the 3D-spheroid implanted group compared to those in the sham, non-implanted, and 2D-hASC implanted groups. Protein levels of RhoA, p-MYPT1, and p-MLC$_{20}$ were higher in the 3D-spheroid-implanted group than in the other groups. At 2 weeks, in the implanted groups, the cryoinjured tissues (which exhibited DiI, α-SMA, and RhoA signals) were restored, while they remained defective in the sham and non-implanted groups.

*Correspondence:
Iltae Son
1tae99@hanmail.net
Sung-Bum Kang
kangsb@snubh.org
Full list of author information is available at the end of the article

Conclusions These findings demonstrate that, compared to 2D-cultured hASCs, 3D-spheroids more effectively induce a contractile phenotype that is initially weak but subsequently improves, inducing expression of RhoA/ROCKII-downstream molecules and SMC differentiation associated with IAS basal tone.

Keywords Adipose stem cell, Smooth muscle cell, Internal anal sphincter, Fecal incontinence, Spheroid

Background

Fecal incontinence (FI), which ultimately leads to involuntary leakage, results from a reduction in the resting pressure of the internal anal sphincter (IAS); this pressure arises from the basal tone generated by smooth muscle cells (SMCs) [1, 2]. Isolation of specific IAS-induced FI phenotypes might be difficult in translational or clinical settings [3, 4]. However, the capacity of stem cells to restore the basal tone required to generate resting pressure, and the mechanisms of this restoration, remain unclear [5–14]. The myogenic features and molecular mechanisms of the IAS required for normal continence differ distinctly from those of the skeletal muscle cells in the external anal sphincter (EAS) [15]. Additionally, the complex multifactorial pathways modulating basal tone in IAS SMCs have recently been discovered and reported [16–24].

Among the molecular subunits responsible for IAS basal tone, the Ras homolog gene family, member A/Rho-associated, coiled-coil containing serine/threonine kinase (RhoA/ROCK) pathway is critical in determining basal tone development [18, 25, 26]. Previous experimental studies using mechanical procedures such as simple division, segmental resection, or crush injury and various cellular treatments of the EAS and IAS have not been able to characterize the contractile phenotype of impaired basal tone in IAS, and data on the resulting molecular changes are lacking [14, 27–32]. Based on our recent systematic review [33], no studies have yet revealed the effects of stem cell therapy on basal tone or examined the pathways that mediate basal tone [14]. Furthermore, cell growth is difficult to achieve in the hazardous serum-free IAS environment, owing to sphincter muscle pressure and fecal passage; a technique is therefore required to enhance cell resistance [14, 34].

As an improvement over two-dimensional (2D) monolayer culturing**,** the three-dimensional (3D) culture technique has been applied to accelerate the translation of cell therapy, achieving "niche" in vivo growth and sufficient cell size to enable the cells to lodge within the muscular interstices [34–36]. Unlike the bidirectional cell–matrix interactions achieved in 2D culture, 3D culture generates omnidirectional interactions, thus generating a more physiological microenvironment via de-novo extracellular matrix (ECM) [37] generation, with the secretion of large amounts of factors [38–40]. Although the potential use of adipose stem cells as cell therapy for FI has been examined [30–32, 41], the use of 3D-culturing for cell therapy has not yet been attempted.

To address this gap, we aimed to develop an in vivo model with myogenic features and a contractile phenotype underlying IAS basal tone and to detect cell-lineage differentiation and phenotype shifting of 3D-spheroids. The results are compared with those obtained using conventional 2D-cultured human adipose stem cells (hASCs). The mechanisms determining the fate of implanted stem cells and modulation of the Rho/ROCK pathway and downstream expression of SMC-related molecules in IAS are examined.

Methods

Study design

We hypothesized that cell lineage differentiation with contractile phenotype shifting occurs following 3D-spheroid implantation. Before examining this in our in vivo model, we conducted an in vitro comparison between 2D-cultured hASCs and 3D-spheroid implantation. Therefore, we first aimed to confirm the differentiability and contractile phenotype of IAS SMCs using 2D- and 3D-cultured hASCs in a smooth muscle cell induction medium. The IAS-targeted FI model was experimentally tested to confirm the specificity of the normal control, sham, and cryoinjured groups. Cell implantation was then conducted using the established in vivo cryoinjured model, in three groups: cryoinjury (non-implantation), 2D-hASC-implantation (2D-hASC group), and 3D-spheroid-implantation (3D-spheroid group). Random allocation of model animals and blinding for data assessment, analysis, and interpretation were conducted for each experiment. Allocation of a normal control group for cell implantation was not possible, owing to the difficulty of blinding during cell implantation.

In vitro pre-processing for cell culture

hASCs, provided by Anterogen Co., Ltd. (Seoul, South Korea) were cultured in MEM α, GlutaMAX supplement containing 0.1% gentamicin, MycoZap Plus-PR, and 10% FBS [14]. The cells were harvested after 2 or 4 weeks to confirm proper differentiation into SMCs, with a change of the medium every 2–3 days. Human adipose-derived stem cells (hADScs) seeded at 1.5×10^5 cells in agarose gel molds (Microtissues 3D Petri Dish; cat. no. 12–81;

Sigma Aldrich, St Louis, MO, USA) were used to generate 3D-spheroids (Additional file 1: Fig. S1a, b). The treatments involved the control (non-treated), 2D-hASCs, and 3D-hASCs cells (all using smooth muscle cell inductive medium), cultured for 2 or 4 weeks, resulting in six groups. After confirmation of differentiation into SMCs, the expression of SMC markers—smooth muscle myosin heavy chain (SMMHC), SM22a, smoothelin, caldesmon, calponin, α-smooth muscle actin (α-SMA), and Rho/ROCK-downstream molecules [RhoA, ROCKII, catalytic 38-kDa type 1 protein phosphatase isoform (PP1c), PKCα, pThr696-MYPT1, total MYPT1, pThr38-CPI-17, total CPI-17, pThr18/Ser19-light chain of myosin$_{20}$ (MLC_{20}), and total MLC_{20}]—was measured with or without 500 nM $CaCl_2$ treatment for 10 min, after 1, 14, and 28 days.

Development of IAS-specific in vivo model

Our previously reported protocol for an IAS-targeted animal model involving intersphincteric dissection [14] was modified using submucosal dissection to reduce unintentional damage to the EAS (the outer longitudinal skeletal muscle layers at the level of the anal canal) during dissection or cryoinjury (Fig. 1a–h). The submucosal dissection depth was reduced to < 1 mm, consistent with the distance from the mucosal surface to the submucosal dissection plane (ca. 500–700 μm), as illustrated via Masson's trichrome staining of a normal anal sphincter (Additional file 1: Fig. S1c, d). The entire sphincter ring was also harvested by dividing it into the proximal and distal ring to identify the anal canal (distal ring) and rectum (proximal ring), as the rectum and IAS differ in the expression of Rho/ROCK and its downstream molecules (Fig. 1f) [26]. Furthermore, to characterize the region of interest (ROI) for the cryoinjured area, part of the ROI was harvested separately to reduce bias in western blotting or PCR analysis owing to the presence of SMCs in uninjured normal tissue (Fig. 1g). These protocol modifications to the dissection plane, ROI generation for cryoinjury, and section division to exclude the rectum were verified using 40 rats in preliminary experiments (Additional files 2, 3).

Dil-stained hASCs (2D-cultured, 1×10^6 cells per site; 3D-spheroids from four molds, using aggregated 1×10^6 cells) were implanted in a carrier (0.5% collagen, 100 μL) at a depth of approximately 250 μm to prevent leakage

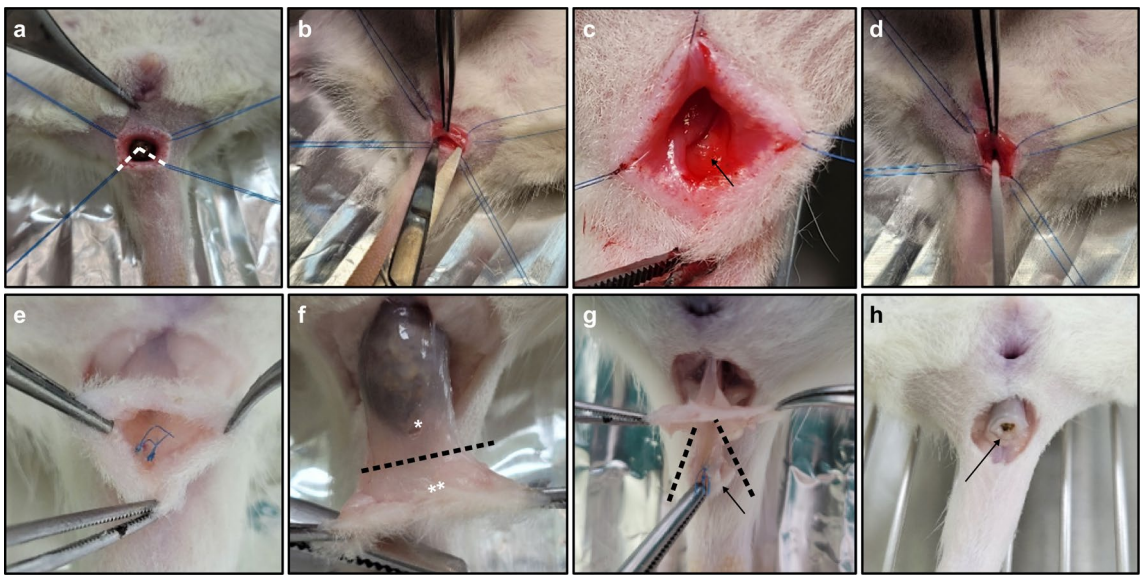

Fig. 1 Methods for internal anal sphincter (IAS)-targeted cryoinjury. Normal anal sphincter of 4-week-old Sprague–Dawley rats, tag sutured at site 4 to indicate the region of interest (ROI) (white dotted line) (**a**). An initial incision above the anal verge was made transversely in the posterior quarter (i.e., at an angle of 125°–215°) of the anal sphincter (**b**). Surgical dissection < 1 mm in depth, along the caudal-to-cranial plane through space (**c**) between the submucosal and muscular layers of the anal sphincter was performed to approach the dorsal surface of the IAS (black arrow) corresponding to the inner circular smooth muscular layer at the level of the anal canal. (**d**) Rapid freezing was applied to the ventral side of the dissected surface confined to the ROI, using an aluminum rod chilled to − 196 °C for 3 s, repeated three times. After cryoinjury, the initial incision was repaired with interrupted non-absorbable sutures. To harvest the site of injury, surgical dissection was performed around the anal sphincter, and the ROI tagging suture was identified in the anal canal (**e**). The entire sphincter ring at the level of the anal canal (**f**) was divided into the proximal sphincter ring (rectum side*), followed by the detachment of the distal ring** at a distance of 2 mm from the proximal ring (dotted line). (**g**) Conical sections of targeted tissue were harvested from the ROI (black arrow) at the height of the tag-sutured area by removal of intact tissue from the entire IAS ring (dotted line). (**h**) The submucosal dissection plane (dotted arrow) was observed between the submucosal and muscular layers after harvesting the entire sphincter

and diffusion of implanted materials (Additional file 1: Fig. S1e, f). Dual staining for α-SMA and RhoA was used to determine whether cells exhibiting α-SMA and RhoA immunofluorescence corresponded with Dil-signal intensity at the injury site. Newly differentiated exogenous SMCs were defined as cells exhibiting consistent immunofluorescence signals for Dil, α-SMA, and RhoA. Owing to fibrosis and fusion between dissection planes, we abolished long-term delayed implantation in our protocol. All experimental procedures were conducted under anesthetic at an appropriate depth using isoflurane anesthesia with an initial dose of 3% and a maintenance dose of 2.5%. After harvesting, carbon dioxide gas was used for euthanasia of all experimental animals.

The dissected and stained tissue was used for hematoxylin and eosin (H&E) staining, immunofluorescence, Masson's trichrome staining, PCR analysis, and western blotting. The gene-specific primers are listed in Additional file 4: Table S1. This animal study was conducted in accordance with the guidelines of and with the approval of the Institutional Animal Care and Use Committee of Hallym University (HMC 2022-1-0609-24).

RNA isolation and quantitative real-time PCR

Total RNA was isolated using easy-BLUE reagent (Intron Biotechnology, Seongnam, Republic of Korea) according to the manufacturer's protocol. Amplification was conducted in a premixture (20 μL) containing 4 μL 5 μM gene-specific primers (Additional file 4: Table S1), 10 μL 2×SYBR, and 6 μL template, under the following conditions: denaturation at 95 °C for 5 min; 40 cycles of 95 °C for 10 s, 59 °C for 34 s; and a final extension at 72 °C for 5 min. PCR products were separated on 2% agarose gels and visualized using ethidium bromide staining.

Western blotting

Cells or tissues were washed twice with ice-cold phosphate-buffered saline (PBS), lysed with an appropriate amount of tissue lysis buffer (RIPA buffer containing protease and phosphatase inhibitor cocktail), incubated on ice for 30 min, and centrifuged at 13,000 rpm for 15 min at 4 °C. Next, 30 μg total protein was loaded and separated using sodium dodecyl sulfate–polyacrylamide gel electrophoresis. Proteins were transferred to polyvinylidene difluoride membranes, blocked for 1 h with 5% nonfat dry milk in Tris-buffered saline (TBS) supplemented with 0.05% Tween-20 (TBS-T), and incubated with the appropriate primary antibodies in TBS-T overnight at 4 °C. Membranes were washed several times with TBS-T and incubated with horseradish peroxidase-conjugated secondary antibodies (0.1 μg/mL; Jackson ImmunoResearch Laboratories, West Grove, PA, USA). Immunoreactivity was detected using an enhanced chemiluminescence detection system (WSE 6100 LuminoGraph I; ATTO, Tokyo, Japan). The band density of western blots was measured using ImageJ (National Institutes of Health, Bethesda, MD, USA) and normalized to those of ERK2 and β-actin as loading controls.

Immunofluorescence staining

Cells grown on round glass coverslips in 24-well plates were fixed and permeabilized with 100% cold methanol for 10 min. Fixed cells were incubated for 1 h in PBS containing 3% bovine serum albumin for blocking, followed by 2 h of incubation with specific primary antibodies. Cells were washed three times with TBS-T, then incubated with Cy2-conjugated goat anti-rabbit/mouse IgGs (Jackson ImmunoResearch Laboratories) or Alexa 594-conjugated goat anti-rabbit/mouse IgGs (Molecular Probes, Eugene, OR, USA) as necessitated by the primary antibody used. Cellular DNA was counterstained with 4′,6-diamidino-2-phenylindole (0.2 μg/mL in PBS).

Hematoxylin & eosin (H&E) staining

Tissues were fixed in 4% phosphate-buffered paraformaldehyde, embedded in paraffin, and sectioned to a thickness of 3 μm. For H&E staining, specimens were dewaxed, rehydrated in an ethanol-graded series, washed twice with PBS, immersed sequentially in hematoxylin and eosin solutions, and dehydrated with two changes of 95% ethanol. Finally, the slides were dehydrated using an ethanol-graded series, incubated with xylene, and mounted with balsam.

Masson's trichrome staining

Masson's trichrome staining (connective tissue staining) was performed according to the manufacturer's instructions (#SS1026-MAB-500, Cancer Diagnostics Inc, Durham, NC, USA). Briefly, cryosection slides were placed in preheated Bouin's fluid for 60 min, followed by a 10 -min cooling period. The slides were rinsed in tap water until the sections were completely clear, then washed once in distilled water. The slides were then stained with equal volumes of Weigert's A and B for 5 min, followed by washing with running tap water for 2 min. Next, the slides were exposed to Biebrich scarlet–acid fuchsin solution for 15 min and rinsed with distilled water. The slides were differentiated in phosphomolybdic/phosphotungstic acid solution until the collagen was no longer red, then rinsed with distilled water. Without further rinsing, the slides were treated with aniline blue solution for 5–10 min, followed by treatment with 1% acetic acid for 3–5 min and rapid dehydration with two changes of ethanol at 95% and 100%, respectively. Finally, the slides were incubated with xylene and mounted with balsam.

Statistical analysis and sample size calculation

Estimation of the allocated experimental unit, analytical procedures, outcome measurements, and reporting methods were in accordance with the ARRIVE 2.0 guidelines [42]. Sample-size estimation (based on the resource equation method [43]) and one-way ANOVA were conducted at each experimental stage based on the a priori-determined effect size [14] and the pooled data presented in our systematic review [25]. To assess whether the data met the assumptions of the statistical approach, two-way ANOVA followed by the post hoc Bonferroni test was applied to the primary outcome measurement data at each experimental stage. To develop the IAS-targeted in vivo model, 60 rats in total were used, categorized into normal, sham, and cryoinjury groups, with tissue harvesting at 1 and 2 weeks. The in vivo cell implantation experiment was performed using 50 rats allocated via simple randomization to cryoinjury (non-implantation), 2D-hASC, and 3D-spheroid implantation groups. Three groups (n = 42 rats in total) with seven rats per group (ANOVA degrees of freedom = 18), were used for tissue harvesting at 1 or 2 weeks, with a normal control group (n = 7) included for reference. The primary outcomes—differentiation into SMCs with shifting of contractile phenotype characterized by expression of Rho/ROCK and its downstream molecules—were compared between the 2D- and 3D-cell implantation in vivo models. GraphPad Prism (9.3.1) (GraphPad Software Inc, San Diego, CA, USA) was used for statistical analyses. Differences with $p < 0.05$ were considered significant.

Results

In vitro experiments

To determine the role of stem cells in the animal model, we examined the capacity of hASCs to differentiate into cells with myogenic profiles corresponding to SMCs in vitro. In the 3D-hASC group, 3D spheroids were embedded within numerous cell populations and were aggregated at the core of each cell population, whereas the 2D-cultured cells were diffused throughout the control medium (Fig. 2a). At 2 and 4 weeks, spindle-like cells were observed, with greater cell proliferation from the aggregated spheroids than from the 2D-cultured hASCs. Immunofluorescence staining of the 3D-ASC group revealed a round shape with a homogenous pattern consistent with the shape of the 3D spheroids, while

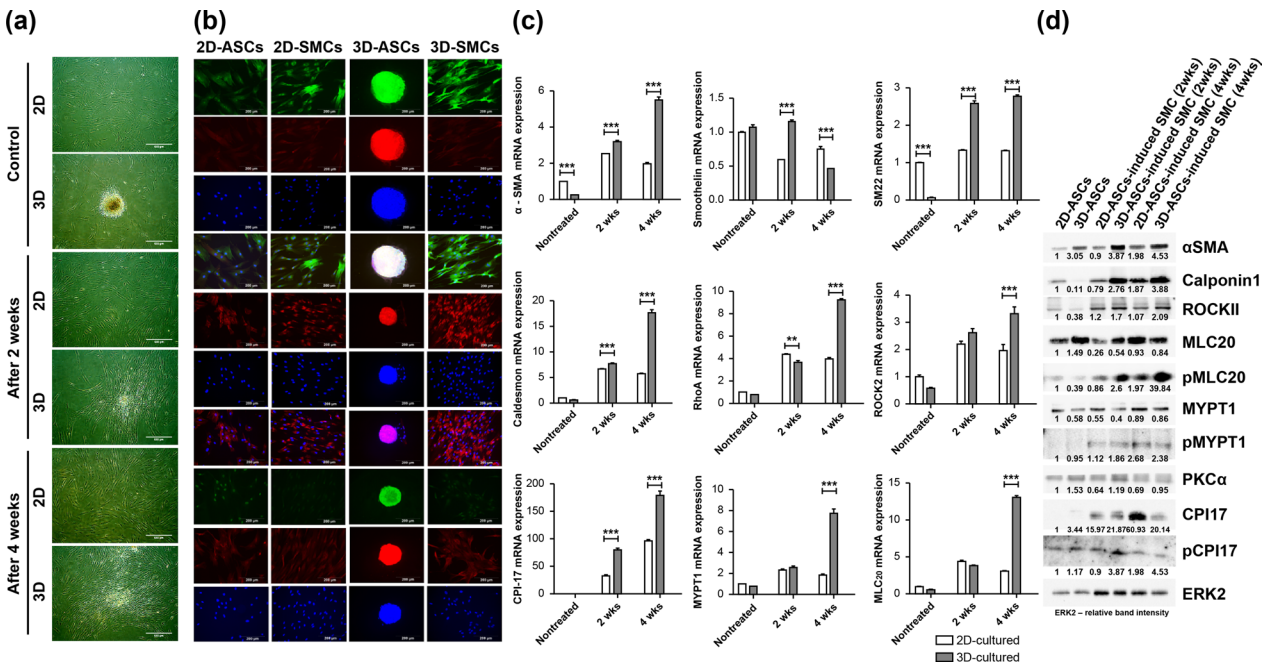

Fig. 2 In vitro proliferation and differentiation. **a** 2D and 3D-cultured adipose stem cells (ASCs) in MEM-α growth medium (control group). In smooth muscle inductive medium, a change in cell population and morphological transformations occurred after 2 and 4 weeks, respectively. **b** Immunofluorescence staining for 2D- and 3D-cultured ASC groups treated with 500 nM $CaCl_2$ for 10 min. 3D-ASCs indicate 3D-spheroid aggregated cells displaying different colors according to specific markers. After differentiation into SMCs, α-SMA, PKCα, $pMLC_{20}$, ROCKII, and RhoA were expressed in 2D and 3D SMC groups. **c** RT-PCR-based mRNA expression (relative to that of *Gapdh*) revealed the expression of *aSma*, caldesmon, *SM22*, smoothelin, caldesmon, *RhoA*, *RockII*, *Mypt1*, *Cpi17*, and Mlc_{20} in the 2D- and 3D-SMC groups after 2 and 4 weeks of differentiation. **d** Western blot images reveal the band intensities (relative to those of ERK2) of the SM proteins, Rho/ROCK, and downstream molecules in the six treatment groups

the 2D-ASC group exhibited diffuse and dispersed patterns (Fig. 2b). At 2 weeks, relative to the 2D-SMC group (i.e., SMCs differentiated from 2D-cultured ASCs), the 3D-SMC group exhibited stronger expression of α-SMA and $pMLC_{20}$, but similar expression of RhoA, ROCKII, and PKCα. Immunofluorescence dual-staining for α-SMA/PKCα and RhoA/ROCKII revealed correlated distributions of the relevant antibodies on the same overlayed tissue sections; in contrast, the distribution of the $pMLC_{20}$/smoothelin antibodies was not correlated with those of the others. Based on western blotting and immunofluorescence, exposure to $CaCl_2$ did not affect protein expression in either of the culture groups. At 4 weeks, *RhoA, RockII, Mypt1, Mlc_{20}, Cp17, aSma,* Caldesmon, and *Sm22* mRNA expression was higher in the 3D-hASC group than that in the 2D-hASC group, whereas at 2 weeks, *RhoA, RockII, Mypt1*, and *Mlc_{20}* expression was lower in the 3D-hASC group than those in the 2D-hASC group (although in some cases the levels were similar). Before cell differentiation, relative to the 2D-cultured hASC group, all markers exhibited similar or even reduced levels (in the control medium) in the 3D-hASC group (Fig. 2c). Western blotting revealed phenotype shifting characterized by α-SMA, calponin, ROCKII, and $pMLC_{20}$ expression, with the highest intensity in 3D-SMCs (Fig. 2d). CPI-17 and pMYPT-1 intensities in the SMC-differentiated groups were also greater than those in the control groups before differentiation.

Development of the in vivo model, cell implantation, and cell tracking

To ensure that only the SM IAS layers exhibited cryoinjury, we attempted to determine whether cryoinjury was limited to the SM layer of the anal sphincter at the level of the anal canal, in the normal control, sham, and, cryoinjury groups. The cryoinjury group, but not the normal control and sham groups, exhibited substantial loss of the third layer (corresponding to the IAS) of the anal canal (Fig. 3a). The cryoinjury-induced ROI (500–900 μm in depth, at an angle of 90° ± 15°) was located at the level of the anal canal (distal section) with squamous epithelial cells layers, and not in the mucosal lining of the rectum (proximal section) consisting of columnar epithelium with crypts (as illustrated through immunofluorescence staining) (d) (Fig. 3b). Based on immunofluorescence staining, submucosal dissection of the ventral side of the cryoinjury revealed IAS tissue dysfunction, characterized by SMC markers and RhoA/ROCKII. Based on RT-PCR, the mRNA expression levels of all markers were lower in the distal than those in the proximal section, indicating that the cryoinjury did not extend to the rectum (Fig. 3c).

At 1 week, immunofluorescence staining to observe the restorative effect of cell implantation on muscle damage in the ROI revealed substantial loss of SM layers, with collateral damage in the ROI in the distal section. However, at 2 weeks, muscular infiltration leading to augmentation was observed in the 2D-hASC and 3D-spheroid implantation groups (Fig. 4a, b), whereas in the untreated cryoinjury group, these defective spaces remained empty at 2 weeks (Fig. 3a). Cell tracking in the ROI of the distal section identified Dil-labeled cells within the augmented muscular tissue (Fig. 4c, d). Those cells were located adjacent to the sites displaying α-SMA and RhoA signals. However, α-SMA and RhoA were not expressed at the same sites, and they exhibited different patterns of enhanced expression in the distal section at 2 weeks.

Based on the RT-PCR analysis results, at 2 weeks, the mRNA expression levels of *aSma, Sm22a,* Smoothelin*, RhoA, Mypt1, Mlc_{20}, Cpi17,* and *Pp1cd* were lower in the sham and cryoinjury groups than those in the 2D-hASCs and 3D-spheroid implantation groups. In contrast, *calponin, caldesmon, SMMHC, ROCKII, PKCα, fibronectin*, and *Col1a1* expression were the highest in the sham group at both 1 and 2 weeks. At 2 weeks, *aSMA*, *Smoothelin*, *MYPT1, MLC_{20},* and *CPI17* expression levels were the lowest in the cryoinjury group.

At week 1, high initial mRNA levels of *calponin*, *SMMHC, caldesmon, Col1a1, FN, ROCKII*, and *PKCα* was observed in sham group. *RhoA* expression was the highest in the 3D-spheroid implantation group. At 2 weeks, *FN*, *Col1a1,* and *ROCKII* expression in the sham groups remained the highest level; however, the cryoinjury group showed the lowest level of *α-SMA* and *MLC_{20}*. The 3D-spheroid implantation group exhibited significantly reduced *FN* and *Col1a1* expression but enhanced *α-SMA, SM22a, smoothelin, RhoA, CPI17,* and *PPI1cd* expression (Fig. 5a).

Western blot analysis showed enhanced expression of FN, ROCKII, PKCα, $pMLC_{20}$ in the sham group at 1 week. In the 2D-ASC or 3D-spheroid implantation group, expression levels of α-SMA, RhoA, ROCKII, p-MYPT1, p-MLC_{20}, PKCα, and p-CPI-17 were weak or lower than those in the other groups at 1 week. However, at 2 weeks, expression levels of RhoA, p-MYPT1, and p-MLC_{20} in the 3D-spheroid implantation groups were substantially higher than those in the other groups. (Fig. 5b).

Discussion

This study presents the first application of an established technique using 3D-spheroids to induce SMCs in an IAS-targeted cryoinjured mouse model. The ability of 3D-spheroids to induce the expression of Rho/ROCK and its downstream molecules was examined. The in vivo model exhibited cell differentiation into SMCs and expression of Rho/ROCKII and other substrates. The cell fate and effects of 3D-spheroids were compared to

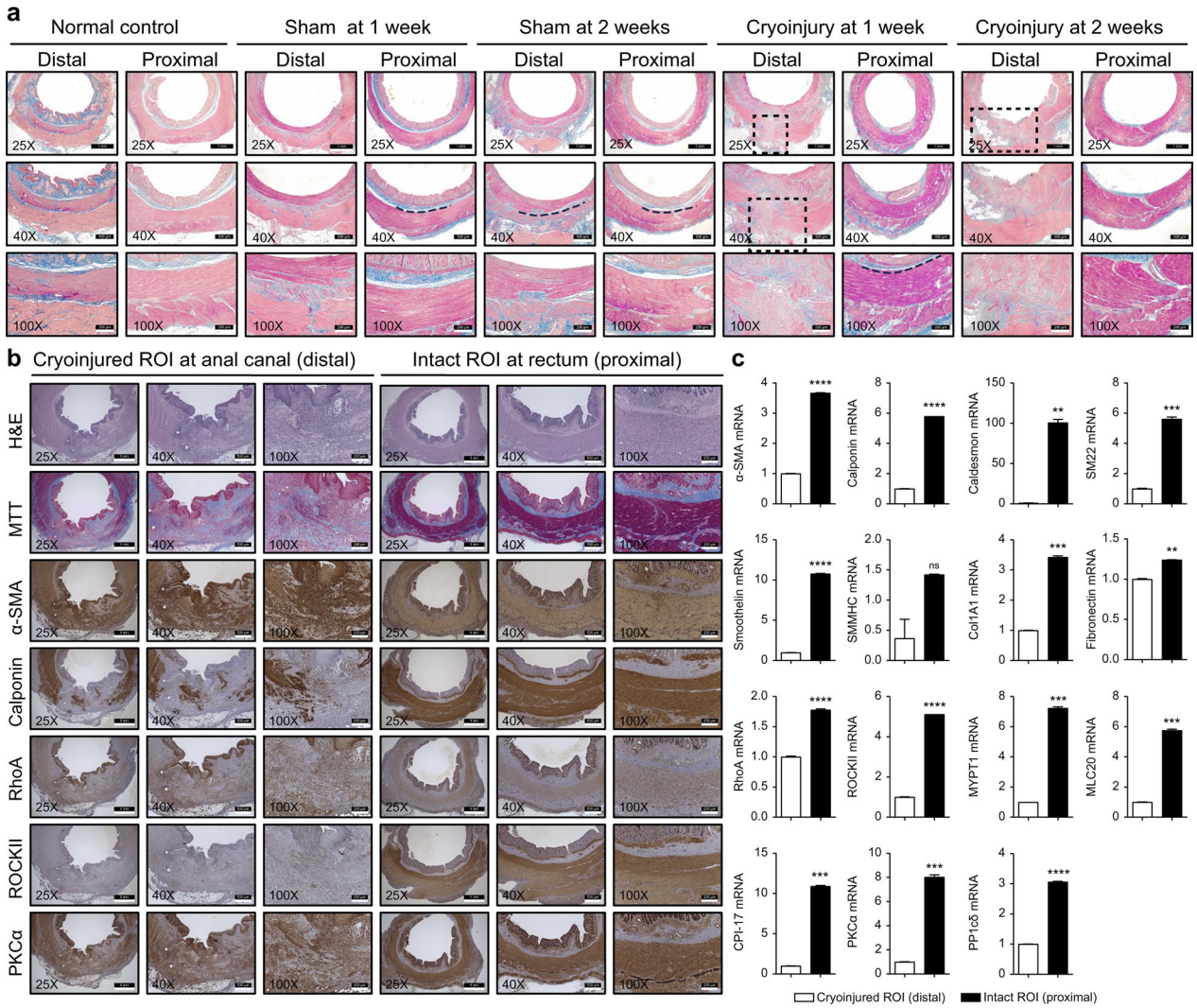

Fig. 3 Development of internal anal sphincter-targeted cryoinjured in vivo model. **a** Normal control groups, exhibiting four layers, namely the epithelium, submucosa, inner circular muscular layers, and cross-sectioned outer longitudinal muscular bundles. The space between the submucosal and muscular layers was observed in both sections. In the sham group, the dorsal submucosal layer (dotted black line) was identified via submucosal dissection in both sections without muscular loss. The submucosal dissection plan of only the distal section showed haziness with muscular infiltration, which was not present in the normal control and proximal section of the sham groups. In the third layer of the distal section of the cryoinjured groups after 1 week, loss of muscular volume within the ROI (dotted box) was observed, whereas the submucosal and muscular layers of the proximal section were intact. The distal section of the ROI still exhibited extensive damage at 2 weeks (dotted box). **b** Staining (hematoxylin and eosin, Masson's trichrome, and immunofluorescence staining with α-SMA, calponin, RhoA, ROCKII, and PKCα of the cryoinjured ROI distal section with epithelial lining comprising squamous cells, corresponding to the anal canal, and intact structure of the proximal section with columnar epithelium with crypts, corresponding to the rectum. **c** mRNA expression of the SMC markers and Rho/ROCK and its downstream molecules (relative to that of *Gapdh*), in the proximal and distal anal sections assessed using RT-PCR

those of conventional 2D-cultured cells. The molecular links between 3D-spheroid implantation and differentiation into SMCs in the injured host IAS were examined in terms of the complex molecular mechanisms underlying basal tone [33].

In vitro, the 3D spheroids initially interacted weakly with the original matrix and induced weak protein expression, but the interaction and induction strength later increased substantially; this is consistent with prior findings [40]. In vivo, the sham might exhibit reversible properties in reaction to the surgery or to tissue renewal from the remaining intact muscular tissue. In contrast to the sham, the cryoinjured models exhibited consistently weak *RhoA, Mypt1,* and Mlc_{20} mRNA expression. This confirms shifting to the contractile phenotype under basal-tone impairment and may explain why this

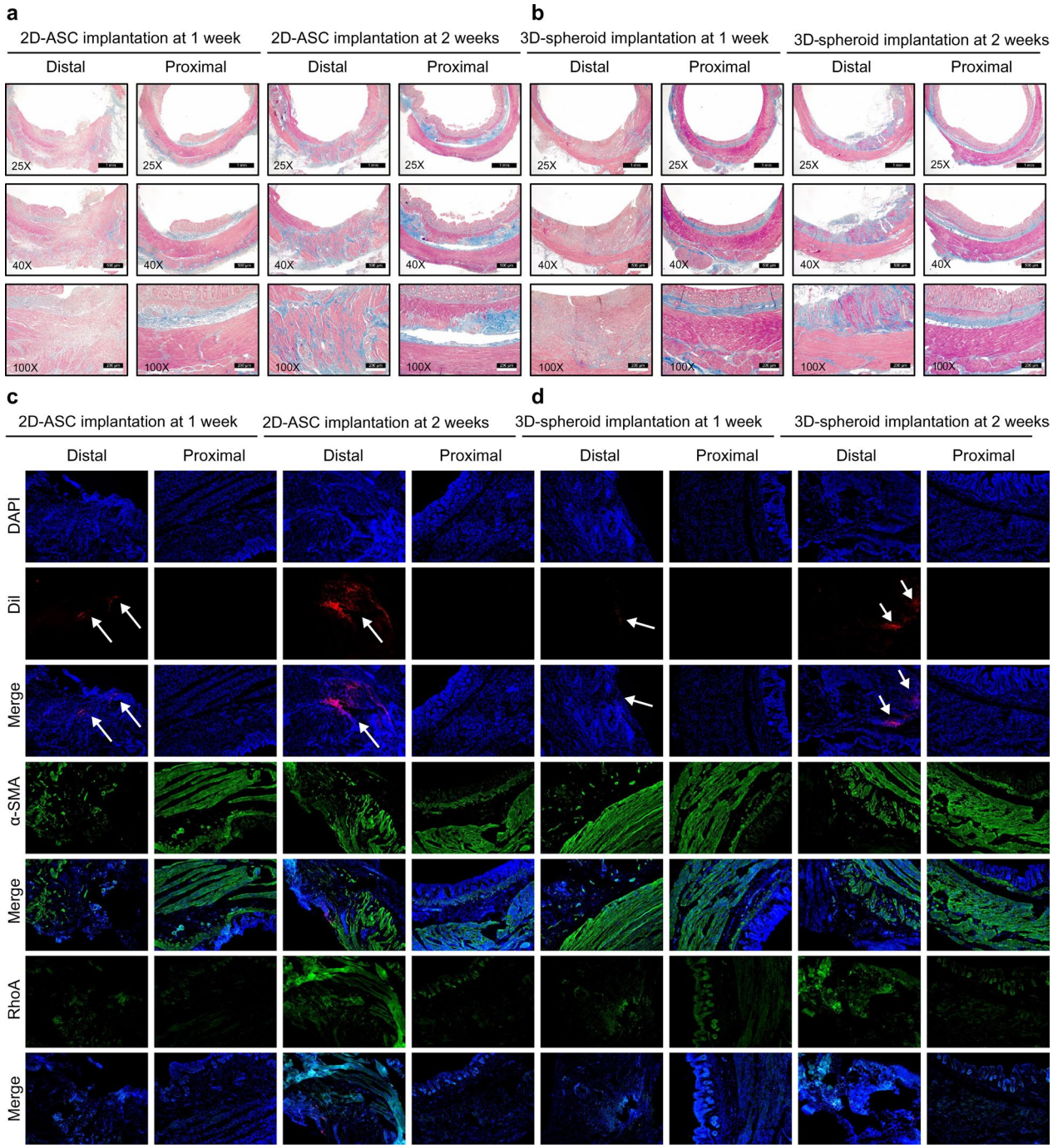

Fig. 4 Staining and tracking of implanted cells in the in vivo model. Masson's trichrome staining for harvest of distal and proximal sections at 1 and 2 weeks after cell implantation of 2D-hASCs (**a**) and 3D-spheroids (**b**) at the cryoinjured site. Cell tracking revealed that DiI-stained 2D- hASCs (**c**) and 3D- spheroids (**d**) were found (white arrow) within only the distal section at 1 and 2 weeks. Merged image of immunofluorescence staining for α-SMA and RhoA revealing the location of DiI-labeled cells adjacent to tissues displaying α-SMA and RhoA signals that were mismatched with the DiI signals in both cases

in vivo IAS-targeted cryoinjured model exhibits more realistic biological features than previous mechanistically induced models [29–34]. On implantation, the 3D-spheroids induced initially weak but strengthening contractile expression of RhoA/ROCK and its downstream molecules, rather than first inducing myogenic

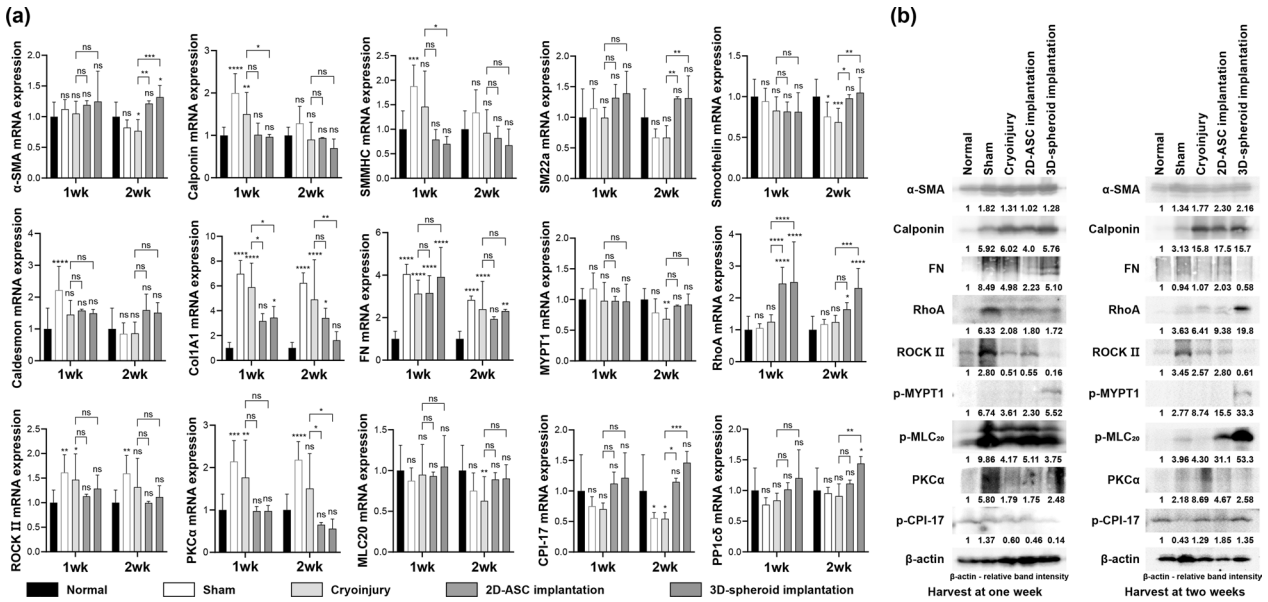

Fig. 5 Outcomes of cell implantation in the in vivo model. **a** mRNA expression (relative to that of GAPDH) determined using PCR and (**b**) band intensities relative to β-actin determined using western blotting for smooth muscle cell differentiation markers, fibrosis markers, and Rho/ROCKII and its downstream molecules in normal, sham, cryoinjury (without cell implantation), and 2D-ASC and 3D-spheroid implantation groups

differentiation of SMCs. This effect may compensate for the cryoinjury-induced loss of *RhoA, Mypt1,* and Mlc_{20} mRNA expression.

Paracrine effects may also reduce fibrosis marker expression substantially more in the 3D-spheroid-treated mice than in the 2D-ASC-treated mice. This may be consistent with our in vitro finding that, after the 3D spheroids become lodged in the 3D environment, interactions between the implanted cells increase as they produce their own matrix and secretory factors, consistent with the behavior of IAS SMCs. Therefore, we infer that contractile-phenotype shifting, characterized by the expression of RhoA/ROCK and its downstream molecules, might be a key molecular mechanism in cell treatment, rather than myogenic differentiation into SMCs. Moreover, it remains unclear whether the hASC differentiation-induced formation of new sphincter muscle tissue is the primary factor leading to healing in anal sphincter repair [44]. Therefore, considering preliminary findings based on a randomized study using hASCs [41], future clinical research using 3D-spheroids could address unresolved issues in cellular therapy.

The patterns of protein expression observed in this cryoinjured IAS model (with cryoinjury at 300–500 μm depth in the SM layers), differed substantially from those observed in previous studies, which reported elevated levels of MYPT1 and reduced levels of RhoA/ROCKII, p-MYPT1, CPI-17, p-CPI-17, and pThr18/Ser19-MLC_{20} [18, 25, 26]. Rapid freezing of the ROI in the IAS ring can induce physicochemical responses, influencing the intactness of the plasma membrane, which binds intracellular Rho/ROCK but not substrates such as MLC and MYPT1 [14, 45–47]. These factors, or insufficient intensity of cryoinjury, might explain why our cryoinjured model did not exhibit a substantial reduction in downstream protein expression. However, at 2 weeks, in the cryoinjured model, reductions were observed in Mlc_{20} and *Cpi17* mRNA levels, along with the levels of SMA-specific markers (α-SMA, SM22a, and smoothelin). Furthermore, the expression fraction of RhoA can be determined by calculating its translocation from the cytosol to the cell membrane in IAS tissue exhibiting basal tone [25]. In the in vitro experiment, the basal tone was not activated, potentially explaining the low in vitro RhoA expression.

Tonic contraction of the IAS can be sustained by preventing or delaying MLC_{20} dephosphorylation; this delay, mediated by the RhoA/ROCK and PKC pathways, is achieved via inhibition of MLCP via the action of PP1c, MYPT1, and a 20-kDa small regulatory subunit (M20) [25]. A rapid shift from tonic to phasic contraction or loss of SM volume in the IAS can lead to dysfunctional basal tone. MYPT1, one of the regulatory units of smooth muscle, is not essential in determining its function [48]; however, it is a major target, and MYPT1-knockout mice exhibited altered contractile phenotype and force [19, 49]. Our IAS-targeting cryoinjured model in vivo exhibited reduced *MYPT1,* $MLC_{20,}$ and SMC marker

expression at 2 weeks. In sham models, initial enhanced expression of FN, RhoA, ROCKII, p-MYPT1, and p-MLC_{20} might be owing to a compensatory physiological response to surgical stress. p-MYPT1 is associated with MLCP dephosphorylation and phasic-tone induction via p-MLC_{20}. Although the precise mechanisms regulating the contractile molecules for basal tone in the IAS-targeting model in vivo remain unclear, our model might be useful in research to regenerate basal tone in FI.

The proteins expressed in our cryoinjured mouse model (including RhoA and several downstream molecules) also participate in pathways involved in aging-related diseases such as aging-associated IAS dysfunction [17, 50, 51]. Nonetheless, our study did not develop an age-related contractile phenotype model. Further, in our model, phenotypic expression was not influenced by Ca^{2+}. However, MLCK activation in IAS SMCs, induced by a global increase in Ca^{2+} via a RyR–TMEM16A–VDCC signaling module, can set the basal tone, as demonstrated using SM-specific MYPT1-knockout and wild-type mice [19].

Here, implantation of 3D-spheroids induced RhoA/ROCKII and some of its downstream molecules, consistent with changes observed when basal tone is impaired. While augmentation of SM tissue may contribute to functional improvement, our findings indicate that contractile-phenotype shifting is essential to restore basal tone. Our findings are consistent with prior reports of similar myogenic expression profiles of RhoA/ROCK, PKC, and CPI-17 in the intrinsically innervated 3D bioengineered ring (3DBR) isolated from the human IAS; in humans, the circular anal sphincter SM, in the resting phase, can generate in vivo basal tone [52–57]. Furthermore, a 3D-spheroid-induced increase in p-MLC_{20} expression might contribute to maintaining basal tone in the later tonic phase or to sustaining contraction by inhibiting MLCP. [18] It has been suggested that the entire molecular machinery of the IAS in humans is geared toward increasing p-MLC_{20} levels, thus inducing basal tone [27]. Furthermore, the capacity of pCPI-17 to inhibit MLCP is several thousand times greater than that of RhoA/ROCK (which was expressed strongly here). Therefore, RhoA, p-MYPT1, MLC_{20}, pCPI-17, and α-SMA might represent key molecular links between cell therapy and dysfunctional IAS resting pressure. However, based on prior complex cellular mechanosensing analysis, these are just a few of the mechanical stimuli that stem cells may experience in vivo [38–40].

In terms of its limitations, our model did not consider neurovascular innervation. However, basal tone, as an intrinsic property of the IAS, is maintained independently of extrinsic neural stimulation [14]. Furthermore, the fact that we used a small sample of harvested tissue from only the cryoinjured part of the anal canal might have been a source of bias in the detection of mRNA or protein. Additionally, we did not perform western blotting to examine the translocation of Rho/ROCK and its downstream molecules to the membrane from the cytosol following activation via signal transduction [27], which may account for the absence of results pertaining to RhoA. During surgery to induce cryoinjury, collateral damage to the adjacent layers of the targeted SM layer of the IAS ring is unavoidable, despite the modifications made to our previous methods [14]. In this study, the dose of implanted 2D and 3D cultured stem cells was not optimized. Long-term functional measurement of muscle tone was not conducted. Given that our study design of xenotransplantation does not eliminate immune evasion completely, it may be unlikely that any implanted cells would still be present at long-term follow-up, despite the use of 3D-spheroids. Furthermore, in the 3D-spheroid-implanted groups, our detection of additional cell populations for cell tracking failed, as the 3D structure of the spheroids was shattered by the cover slides or by bleaching. Despite the potential for adipogenesis, osteogenesis, and chondrogenesis after stem cell implantation, this study was technically designed to exclude heterogeneous differentiation using high-throughput methodologies, such as human surgical procedures.

Conclusion

In this novel application of 3D-spheroids to induce SMCs in an IAS-targeted cryoinjured mouse model, 3D-spheroid implantation induced contractile phenotype shifting that strengthened over time, as well as the SMC myogenic differentiation required for basal tone in the IAS. These findings identify molecules downstream of RhoA/ROCKII as potential targets for improving dysfunctional basal tone and support advancements in treatment strategies for FI.

Abbreviations

α-SMA	α-Smooth muscle actin
FI	Fecal incontinence
FN	Fibronectin
IAS	Internal anal sphincter
EAS	External anal sphincter
SMC	Smooth muscle cell
SMMHC	Smooth muscle myosin heavy chain
TGF-β	Transforming growth factor β
SM22α	Smooth muscle 22α
RhoA	Ras homolog family member A
ROCKII	Rho-associated coiled-coil containing protein kinase II
MYPT1	Myosin phosphatase target subunit 1
CPI-17	Phosphoprotein inhibitor-17
MLC_{20}	Myosin light chain 20
PP1cδ	Protein phosphatase 1 regulatory subunit
PKCα	Protein kinase C alpha

Supplementary Information

The online version contains supplementary material available at https://doi.org/10.1186/s13287-024-03978-9.

Additional file 1: Fig. S1. Cell preparation and implantation for the internal anal sphincter via submucosal approach. 2D-cultured hASCs in MEM-α medium were seeded at 1.5×10^5 cells/well in fibronectin-coated 60-mm culture dishes and incubated in expansion medium. The next day, for SMC differentiation, the medium was exchanged for either smooth muscle induction medium, MCDB 131 medium supplemented with 1% FBS and 100 units/mL heparin, or low-glucose DMEM containing 0.1% gentamicin and 5 ng/mL transforming growth factor β [TGF-β]). **a** hADSCs seeded in agarose gels. 3D-spheroids were prepared as follows; 2% agarose solution in 0.9% saline solution was prepared using a microwave oven; 500 µL of molten agarose was pipetted into 12-series micromolds for casting into MicroTissues 3D Petri dishes. After the agarose gel set, the micromolds were carefully flexed to remove the MicroTissues 3D Petri dishes. To equilibrate the MicroTissues 3D Petri dishes, we added cell culture medium to 3×10^5 cells in a 100 mm FN-coated dish, 1.5×10^5 cells in a 60 mm fibronectin-coated dish, or 1.5×10^4 cells in a fibronectin-coated 24-well plate), followed by incubation for at least 20 min. The medium was then replaced with fresh medium, and the dishes were incubated again for at least 20 min. Excess culture medium was carefully removed, and 190 µL of the cell suspension was seeded onto MicroTissues 3D Petri dishes, which were then incubated at 37 °C in a humidified 5% CO_2 atmosphere for 3 d. **b** 3D-spheroids in smooth muscle inductive medium. **c** The level and depth of the initial incision was as follows: level of the initial incisionat the anal verge, with squamous epithelial cell layers. **d** Planned submucosal dissection, located above the inner circular muscular layers at the level of the anal canal, with Masson's trichrome-stained squamous epithelial cell layers. After confirming no difference in the relative spheroid length between non-Dil-stained and Dil-stained, 3D-spheroids from four molds using 1×10^5 cells, stained 3D-spheroids (**e**) were implanted starting from the core and proceeding outward **f**.

Additional file 2: **Fig. S2**. Original full-length uncropped western blots of main Fig. 2d.

Additional file 3: **Fig. S3**. Original full-length uncropped western blots of main Fig. 5.

Additional file 4: **Table S1**. Primers.

Acknowledgements
Not applicable

Author contributions
ITS and SBK conceived this study and wrote the manuscript. MK, BYO, and WC supervised this study. MK, JSL, JHP, DY, YRK, and ITS performed the experiments. ITS and JSL conducted the analysis. ITS and SBK revised the manuscript. All authors have read and approved the final manuscript.

Funding
This study was supported by the Basic Science Research Program through the National Research Foundation of Korea (NRF) funded by the Ministry of Education (2022R1I1A3063876) for the period 2022 to 2025.

Availability of data and materials
The data that support the findings of this study are available from the corresponding authors upon reasonable request.

Declarations

Ethics approval and consent to participate
The project titled "Differentiation of human adipose stem cells 3D-spheroids into smooth muscle cells and activation of Rho/ROCK pathway in internal anal sphincter-targeting fecal incontinence animal model" has been approved by the Institutional Animal Care and Use Committee of Hallym University. The approval number for the project is HMC 2022-1-0609-24, and the initial date of approval was 09, June 2022, with an update on 30, May 2023. Furthermore, Anterogen Co., Ltd. (Seoul, South Korea) provided the original source of human adipose stem cells. We declare that Anterogen Co., Ltd had ethical approval for collecting human cells, and the donors had signed informed consent. The Ministry of Food and Drug Safety provided the information on human adipose stem cells, Cupistem®(https://www.mfds.go.kr/eng/brd/m_30/view.do?seq=71337&srchFr=&srchTo=&srchWord=&srchTp=&itm_seq_1=0&itm_seq_2=0&multi_itm_seq=0&company_cd=&company_nm=&page=1).

Consent for publication
Not applicable.

Competing interests
The authors declare that they have no competing interests.

Author details
[1]Department of Surgery, Hallym Sacred Heart Hospital, Hallym University College of Medicine, 22 Gwanpyeong-Ro 170 Beon-Gil, Pyeongan-Dong, Dongan-Gu, Anyang, Gyeonggi-Do, Republic of Korea. [2]Institute for Regenerative Medicine, Hallym Sacred Heart Hospital, Hallym University College of Medicine, Anyang, Republic of Korea. [3]Burn Institute, Hangang Sacred Heart Hospital, Hallym University College of Medicine, Seoul, Republic of Korea. [4]Department of Surgery, Hangang Sacred Heart Hospital, Hallym University College of Medicine, Seoul, Republic of Korea. [5]Department of Surgery, Seoul National University Bundang Hospital, 166 Gumi-Ro, Bundang-Gu, 463-707 Seongnam, Republic of Korea.

Received: 17 April 2024 Accepted: 6 October 2024
Published online: 12 October 2024

References

1. Murthy KS. Signaling for contraction and relaxation in smooth muscle of the gut. Annu Rev Physiol. 2006;68:345–74. https://doi.org/10.1146/annurev.physiol.68.040504.094707.
2. Meyer I, Blanchard CT, Markland AD, Gibson EG, Richter HE. Fecal incontinence symptoms and impact in older versus younger women seeking care. Dis Colon Rectum. 2019;62:733–8. https://doi.org/10.1097/DCR.0000000000001353.
3. Evers J, Jones JFX, O'Connell PR. Systematic review of animal models used in research of origins and treatments of fecal incontinence. Dis Colon Rectum. 2017;60:614–26. https://doi.org/10.1097/DCR.0000000000000841.
4. De Ligny WR, Kerkhof MH, Ruiz-Zapata AM. Regenerative medicine as a therapeutic option for fecal incontinence: a systematic review of preclinical and clinical studies. Am J Obstet Gynecol. 2019;220:142-154.e2. https://doi.org/10.1016/j.ajog.2018.09.009.
5. Frudinger A, Kölle D, Schwaiger W, Pfeifer J, Paede J, Halligan S. Muscle-derived cell injection to treat anal incontinence due to obstetric trauma: pilot study with 1 year follow-up. Gut. 2010;59:55–61. https://doi.org/10.1136/gut.2009.181347.
6. Frudinger A, Pfeifer J, Paede J, Kolovetsiou-Kreiner V, Marksteiner R, Halligan S. Autologous skeletal-muscle-derived cell injection for anal incontinence due to obstetric trauma: a 5-year follow-up of an initial study of 10 patients. Colorectal Dis. 2015;17:794–801. https://doi.org/10.1111/codi.12947.
7. Bisson A, Fréret M, Drouot L, Jean L, Le Corre S, Gourcerol G, et al. Restoration of anal sphincter function after myoblast cell therapy in incontinent rats. Cell Transplant. 2015;24:277–86. https://doi.org/10.3727/096368913X674053.
8. Romaniszyn M, Rozwadowska N, Nowak M, Malcher A, Kolanowski T, Walega P, et al. Successful implantation of autologous muscle-derived stem cells in treatment of faecal incontinence due to external sphincter rupture. Int J Colorectal Dis. 2013;28:1035–6. https://doi.org/10.1007/s00384-013-1692-y.
9. Romaniszyn M, Rozwadowska N, Malcher A, Kolanowski T, Walega P, Kurpisz M. Implantation of autologous muscle-derived stem cells in treatment of fecal incontinence: results of an experimental pilot study. Tech Coloproctol. 2015;19:685–96. https://doi.org/10.1007/s10151-015-1351-0.

10. Frudinger A, Marksteiner R, Pfeifer J, Margreiter E, Paede J, Thurner M. Skeletal muscle-derived cell implantation for the treatment of sphincter-related faecal incontinence. Stem Cell Res Ther. 2018;9:233. https://doi.org/10.1186/s13287-018-0978-y.
11. Kajbafzadeh AM, Elmi A, Talab SS, Esfahani SA, Tourchi A. Functional external anal sphincter reconstruction for treatment of anal incontinence using muscle progenitor cell auto grafting. Dis Colon Rectum. 2010;53:1415–21. https://doi.org/10.1007/DCR.0b013e3181e53088.
12. Kajbafzadeh AM, Kajbafzadeh M, Sabetkish S, Sabetkish N, Tavangar SM. Tissue-engineered external anal sphincter using autologous myogenic satellite cells and extracellular matrix: functional and histological studies. Ann Biomed Eng. 2016;44:1773–84. https://doi.org/10.1007/s10439-015-1468-3.
13. Boyer O, Bridoux V, Giverne C, Bisson A, Koning E, Leroi AM, et al. Autologous myoblasts for the treatment of fecal incontinence: results of a phase 2 randomized placebo-controlled study (MIAS). Ann Surg. 2018;267:443–50. https://doi.org/10.1097/SLA.0000000000002268.
14. Kim M, Oh BY, Lee JS, Yoon D, Kim YR, Chun W, et al. Differentiation of adipose-derived stem cells into smooth muscle cells in an internal anal sphincter-targeting anal incontinence rat model. J Clin Med. 2023;12:1632. https://doi.org/10.3390/jcm12041632.
15. Son IT, Lee HS, Ihn MH, Lee KH, Kim DW, Lee KW, et al. Isolation of internal and external sphincter progenitor cells from the human anal sphincter with or without radiotherapy. Colorectal Dis. 2019;21:38–47. https://doi.org/10.1111/codi.14351.
16. Lu P, Chen J, Zhang C, Saur D, Baer CE, Lifshitz LM, et al. Oscillating calcium signals in smooth muscle cells underlie the persistent basal tone of internal anal sphincter. J Cell Physiol. 2021;236:5937–52. https://doi.org/10.1002/jcp.30279.
17. Singh A, Rattan S. BDNF rescues aging-associated internal anal sphincter dysfunction. Am J Physiol Gastrointest Liver Physiol. 2021;321:G87-97. https://doi.org/10.1152/ajpgi.00090.2021.
18. Rattan S. Ca2+/calmodulin/MLCK pathway initiates, and RhoA/ROCK maintains, the internal anal sphincter smooth muscle tone. Am J Physiol Gastrointest Liver Physiol. 2017;312:G63–6. https://doi.org/10.1152/ajpgi.00370.2016.
19. Zhang CH, Wang P, Liu DH, Chen CP, Zhao W, Chen X, et al. The molecular basis of the genesis of basal tone in internal anal sphincter. Nat Commun. 2016;7:11358. https://doi.org/10.1038/ncomms11358.
20. Cobine CA, Sotherton AG, Peri LE, Sanders KM, Ward SM, Keef KD. Nitrergic neuromuscular transmission in the mouse internal anal sphincter is accomplished by multiple pathways and postjunctional effector cells. Am J Physiol Gastrointest Liver Physiol. 2014;307:G1057–72. https://doi.org/10.1152/ajpgi.00331.2014.
21. de Godoy MA, Rattan N, Rattan S. COX-1 vs. COX-2 as a determinant of basal tone in the internal anal sphincter. Am J Physiol Gastrointest Liver Physiol. 2009;296:G219-25. https://doi.org/10.1152/ajpgi.90485.2008.
22. Rattan S, Regan RF, Patel CA, De Godoy MA. Nitric oxide not carbon monoxide mediates nonadrenergic noncholinergic relaxation in the murine internal anal sphincter. Gastroenterology. 2005;129:1954–66. https://doi.org/10.1053/j.gastro.2005.08.050.
23. de Godoy MA, Rattan S. Translocation of AT1- and AT2-receptors by higher concentrations of angiotensin II in the smooth muscle cells of rat internal anal sphincter. J Pharmacol Exp Ther. 2006;319:1088–95. https://doi.org/10.1124/jpet.106.108084.
24. Singh J, Kumar S, Rattan S. Bimodal effect of oxidative stress in internal anal sphincter smooth muscle. Am J Physiol Gastrointest Liver Physiol. 2015;309:G292-300. https://doi.org/10.1152/ajpgi.00125.2015.
25. Patel CA, Rattan S. Cellular regulation of basal tone in internal anal sphincter smooth muscle by RhoA/ROCK. Am J Physiol Gastrointest Liver Physiol. 2007;292:G1747–56. https://doi.org/10.1152/ajpgi.00438.2006.
26. Rattan S, Singh J. RhoA/ROCK pathway is the major molecular determinant of basal tone in intact human internal anal sphincter. Am J Physiol Gastrointest Liver Physiol. 2012;302:G664–75. https://doi.org/10.1152/ajpgi.00430.2011.
27. Salcedo L, Mayorga M, Damaser M, Balog B, Butler R, Penn M, et al. Mesenchymal stem cells can improve anal pressures after anal sphincter injury. Stem Cell Res. 2013;10:95–102. https://doi.org/10.1016/j.scr.2012.10.002.
28. Salcedo L, Penn M, Damaser M, Balog B, Zutshi M. Functional outcome after anal sphincter injury and treatment with mesenchymal stem cells. Stem Cells Transl Med. 2014;3:760–7. https://doi.org/10.5966/sctm.2013-0157.
29. Oh HK, Lee HS, Lee JH, Oh SH, Lim JY, Ahn S, et al. Functional and histological evidence for the targeted therapy using biocompatible polycaprolactone beads and autologous myoblasts in a dog model of fecal incontinence. Dis Colon Rectum. 2015;58:517–25. https://doi.org/10.1097/DCR.0000000000000346.
30. Inoue Y, Fujita F, Yamaguchi I, Kinoe H, Kawahara D, Sakai Y, et al. Improvement of anal function by adipose-derived stem cell sheets. Dig Surg. 2018;35:64–9. https://doi.org/10.1159/000475475.
31. Kuismanen K, Juntunen M, Narra Girish N, Tuominen H, Huhtala H, Nieminen K, et al. Functional outcome of human adipose stem cell injections in rat anal sphincter acute injury model. Stem Cells Transl Med. 2018;7:295–304. https://doi.org/10.1002/sctm.17-0208.
32. Sarveazad A, Babahajian A, Yari A, Rayner CK, Mokhtare M, Babaei-Ghazani A, et al. Combination of laser and human adipose-derived stem cells in repair of rabbit anal sphincter injury: a new therapeutic approach. Stem Cell Res Ther. 2019;10:367. https://doi.org/10.1186/s13287-019-1477-5.
33. Kim M, Oh BY, Lee JS, Yoon D, Chun W, Son IT. A systematic review of translation and experimental studies on internal anal sphincter for fecal incontinence. Ann Coloproctol. 2022;38:183–96. https://doi.org/10.3393/ac.2022.00276.0039.
34. Cheng NC, Chen SY, Li JR, Young TH. Short-term spheroid formation enhances the regenerative capacity of adipose-derived stem cells by promoting stemness, angiogenesis, and chemotaxis. Stem Cells Transl Med. 2013;2:584–94. https://doi.org/10.5966/sctm.2013-0007.
35. Sart S, Tsai AC, Li Y, Ma T. Three-dimensional aggregates of mesenchymal stem cells: cellular mechanisms, biological properties, and applications. Tissue Eng Part B Rev. 2014;20:365–80. https://doi.org/10.1089/ten.TEB.2013.0537.
36. Bartosh TJ, Ylöstalo JH, Mohammadipoor A, Bazhanov N, Coble K, Claypool K, et al. Aggregation of human mesenchymal stromal cells (MSCs) into 3D spheroids enhances their antiinflammatory properties. Proc Natl Acad Sci U S A. 2010;107:13724–9. https://doi.org/10.1073/pnas.1008117107.
37. Ambriz X, de Lanerolle P, Ambrosio JR. The mechanobiology of the actin cytoskeleton in stem cells during differentiation and interaction with biomaterials. Stem Cells Int. 2018;2018:2891957. https://doi.org/10.1155/2018/2891957.
38. Hyväri L, Ojansivu M, Juntunen M, Kartasalo K, Miettinen S, Vanhatupa S. Focal adhesion kinase and ROCK signaling are switch-like regulators of human adipose stem cell differentiation towards osteogenic and adipogenic lineages. Stem Cells Int. 2018;2018:2190657. https://doi.org/10.1155/2018/2190657.
39. Riento K, Ridley AJ. ROCKS: Multifunctional kinases in cell behaviour. Nat Rev Mol Cell Biol. 2003;4:446–56. https://doi.org/10.1038/nrm1128.
40. Lv H, Li L, Sun M, Zhang Y, Chen L, Rong Y, et al. Mechanism of regulation of stem cell differentiation by matrix stiffness. Stem Cell Res Ther. 2015;6:103. https://doi.org/10.1186/s13287-015-0083-4.
41. Sarveazad A, Newstead GL, Mirzaei R, Joghataei MT, Bakhtiari M, Babahajian A, et al. A new method for treating fecal incontinence by implanting stem cells derived from human adipose tissue: preliminary findings of a randomized double-blind clinical trial. Stem Cell Res Ther. 2017;8:40. https://doi.org/10.1186/s13287-017-0489-2.
42. Percie du Sert N, Ahluwalia A, Alam S, Avey MT, Baker M, Browne WJ, et al. Reporting animal research: Explanation and elaboration for the ARRIVE Guidelines 2.0. PLOS Biol. 2020;18:e3000411. https://doi.org/10.1371/journal.pbio.3000411
43. Charan J, Kantharia ND. How to calculate sample size in animal studies? J Pharmacol Pharmacother. 2013;4:303–6. https://doi.org/10.4103/0976-500X.119726.
44. El-Said MM, Emile SH. Comment on "A new method for treating fecal incontinence by implanting stem cells derived from human adipose tissue: preliminary findings of a randomized double-blind clinical trial." Stem Cell Res Ther. 2018;9:115. https://doi.org/10.1186/s13287-018-0875-4.
45. Truebestein L, Elsner DJ, Fuchs E, Leonard TA. A molecular ruler regulates cytoskeletal remodelling by the Rho kinases. Nat Commun. 2015;6:10029. https://doi.org/10.1038/ncomms10029.
46. Gao D, Critser JK. Mechanisms of cryoinjury in living cells. ILAR J. 2000;41:187–96. https://doi.org/10.1093/ilar.41.4.187.

47. Kang SB, Lee HN, Lee JY, Park JS, Lee HS, Lee JY. Sphincter contractility after muscle-derived stem cells autograft into the cryoinjured anal sphincters of rats. Dis Colon Rectum. 2008;51:1367–73. https://doi.org/10.1007/s10350-008-9360-y.
48. Dirksen WP, Vladic F, Fisher SA. A myosin phosphatase targeting subunit isoform transition defines a smooth muscle developmental phenotypic switch. Am J Physiol Cell Physiol. 2000;278:C589-600. https://doi.org/10.1152/ajpcell.2000.278.3.C589.
49. He WQ, Qiao YN, Peng YJ, Zha JM, Zhang CH, Chen C, et al. Altered contractile phenotypes of intestinal smooth muscle in mice deficient in myosin phosphatase target subunit 1. Gastroenterology. 2013;1465.e1–5;144:1456–65. https://doi.org/10.1053/j.gastro.2013.02.045
50. Singh J, Boopathi E, Addya S, Phillips B, Rigoutsos I, Penn RB, et al. Aging-associated changes in microRNA expression profile of internal anal sphincter smooth muscle: Role of microRNA-133a. Am J Physiol Gastrointest Liver Physiol. 2016;311:G964–73. https://doi.org/10.1152/ajpgi.00290.2016.
51. Singh A, Mohanty I, Singh J, Rattan S. BDNF augments rat internal anal sphincter smooth muscle tone via RhoA/ROCK signaling and nonadrenergic noncholinergic relaxation via increased NO release. Am J Physiol Gastrointest Liver Physiol. 2020;318:G23-33. https://doi.org/10.1152/ajpgi.00247.2019.
52. Hecker L, Baar K, Dennis RG, Bitar KN. Development of a three-dimensional physiological model of the internal anal sphincter bioengineered in vitro from isolated smooth muscle cells. Am J Physiol Gastrointest Liver Physiol. 2005;289:G188–96. https://doi.org/10.1152/ajpgi.00335.2004.
53. Somara S, Gilmont RR, Dennis RG, Bitar KN. Bioengineered internal anal sphincter derived from isolated human internal anal sphincter smooth muscle cells. Gastroenterology. 2009;137:53–61. https://doi.org/10.1053/j.gastro.2009.03.036.
54. Hashish M, Raghavan S, Somara S, Gilmont RR, Miyasaka E, Bitar KN, et al. Surgical implantation of a bioengineered internal anal sphincter. J Pediatr Surg. 2010;45:52–8. https://doi.org/10.1016/j.jpedsurg.2009.10.010.
55. Raghavan S, Miyasaka EA, Hashish M, Somara S, Gilmont RR, Teitelbaum DH, et al. Successful implantation of physiologically functional bioengineered mouse internal anal sphincter. Am J Physiol Gastrointest Liver Physiol. 2010;299:G430–9. https://doi.org/10.1152/ajpgi.00269.2009.
56. Raghavan S, Gilmont RR, Miyasaka EA, Somara S, Srinivasan S, Teitelbaum DH, et al. Successful implantation of bioengineered, intrinsically innervated, human internal anal sphincter. Gastroenterology. 2011;141:310–9. https://doi.org/10.1053/j.gastro.2011.03.056.
57. Raghavan S, Miyasaka EA, Gilmont RR, Somara S, Teitelbaum DH, Bitar KN. Perianal implantation of bioengineered human internal anal sphincter constructs intrinsically innervated with human neural progenitor cells. Surgery. 2014;155:668–74. https://doi.org/10.1016/j.surg.2013.12.023.

Publisher's Note